Stationarity of Multiband Channels for OTFS-Based Intelligent Transportation Systems

Danilo Radovic*, Faruk Pasic*, Markus Hofer†, Thomas Zemen†, Christoph F. Mecklenbräuker*
*Institute of Telecommunications, TU Wien, Vienna, Austria
†Center for Digital Safety & Security, AIT Austrian Institute of Technology GmbH, Vienna, Austria
danilo.radovic@tuwien.ac.at

***Abstract*—The development of communication systems for intelligent transportation systems (ITS) relies on their performance in high-mobility scenarios. Such scenarios introduce rapid fluctuations in wireless channel properties. As a promising solution for vehicle-to-everything (V2X) communication, the orthogonal time frequency space (OTFS) approach has emerged. Nevertheless, the performance of OTFS systems is closely tied to time- and frequency diversity of the wireless propagation channel. However, there is a lack of understanding of the stationarity of the wireless channels, especially in the millimeter wave (mmWave) frequency bands. In this paper, we address this research gap by conducting a comprehensive stationarity analysis of measured sub-6 GHz and mmWave high-speed wireless channels. We evaluate the spatial stationarity of a scenario, where the transmitter is moving at high velocity. Furthermore, we investigate the influence of the transmit antenna orientation on the channel spatial stationarity. We could show that the spatial stationarity is proportional to the wavelength.**

***Index Terms*—V2X communications, sub-6 GHz, mmWave, OTFS, WSSUS, ITS**

I. Introduction

Development of new technologies in the field of intelligent transportation systems (ITS) is seen as one of the major methods to increase the safety and efficiency of passenger and freight transport. These new technologies require wireless connectivity to exchange large amounts of sensor data between users in real-time, thus achieving expanded situational awareness [1]. However, exchanging large amounts of data requires large bandwidths (high data rates) that are not available in the traditionally utilized sub-6 GHz frequency bands. This is the motivation to employ the less congested millimeter wave (mmWave) band for vehicle-to-everything (V2X) communication systems, offering rich available spectrum resources.

High-mobility scenarios, present in vehicular communication, pose significant challenges due to high Doppler spread, and thus fast time varying channel impulse responses [2]. To address challenges posed by time-varying channels, the orthogonal time frequency space (OTFS) modulation [3], [4] and other two-dimensional spreading schemes [5] have been proposed instead of traditionally utilized orthogonal frequency-division multiplexing (OFDM). OTFS outperforms OFDM [6] by exploiting time- and frequency-diversity of a doubly-dispersive channel since its basis functions basically act as a two-dimensional spreading sequence in time and frequency. However, achieving the full potential of OTFS is dependent on the channel properties and the selected time-frequency symbol dimensions [7]. Since the dimensionality of an OTFS symbol is limited by the channel statistics, it is of high interest to evaluate the maximum transmitter (TX) spatial shift for which channel statistics can be approximated as invariant, meaning the channel is stationary. This spatial shift provides us with limits for validity of the OTFS symbol parametrization.

Channel stationarity evaluations for vehicular scenarios in sub-6 GHz [8], [9], demonstrate the dependency of stationarity on the observed scenario. Recent studies of the stationarity in the mmWave vehicular channels are presented in [10], [11]. While [10] provides an investigation of the 28 GHz band, measured in a highway scenario, [11] presents the results of the stationarity in the 60 GHz frequency band in an urban scenario. These investigations provide an initial understanding of the stationarity for dynamic scenarios, across multiple frequency bands. However, since channel stationarity is strongly linked to the observed scenario, conducting comparable stationarity investigation of multiple frequency bands requires the investigation of multi-band measurements within the same scattering environment. The first multi-band stationarity investigation for high-velocity scenario is given [12], suggesting shorter stationarity time in mmWave compared to sub-6 GHz channels. We identify a research gap in the study of spatial stationarity for dynamic multi-band channels and highlight the need to define and explain parameters influencing channel stationarity.

Contribution: In this paper, we investigate the spatial stationarity of measured high-mobility multi-band channels. We present a method to evaluate the stationarity of the channels measured while the TX is moving at high velocity along the predefined trajectory. The stationarity evaluation is performed by estimating the Doppler spectral density (DSD) variation, occurring when the axis of the TX trajectory is shifted in the spatial domain. We evaluate the maximum spatial offset of the predefined TX trajectory for which the channel statistics stay approximately constant. Furthermore, we evaluate the influence of the antenna orientation on the channel spatial stationarity.

The work of D. Radovic, F. Pasic and C. F. Mecklenbräuker was supported by the Austrian Research Promotion Agency (FFG) via the research project Intelligent Intersection (ICT of the Future, Grant 880830). The work of M. Hofer and T. Zemen is supported within the Principal Scientist grant Dependable Wireless 6G Communication Systems (DEDICATE 6G) at the AIT Austrian Institute of Technology.

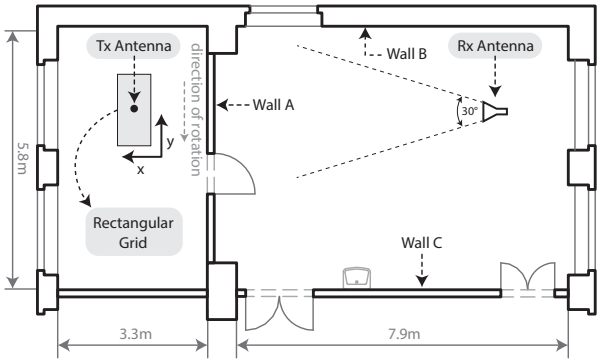

Fig. 1: Measurement laboratory environment.

Notation: Bold uppercase letters denote matrices such as $\mathbf{A}$ and bold lower case letters denote vectors such as $\mathbf{a}$. By $A[u,v]$ and $a[u]$ we denote $(u,v)^{\text{th}}$ and u^{th} element of a matrix and vector, respectively. All-ones matrix is denoted by $\mathbf{1}$ and discrete Fourier transform (DFT) matrix by $\mathbf{F}$, with the dimension given as an uppercase letter in the subscript. Hadamard product is denoted via the operator $\odot$. Frobenius inner product and Frobenius norm are denoted as $\langle \mathbf{A}, \mathbf{B} \rangle_{\text{F}} = \sum_{u,v} A^*[u,v]B[u,v]$ and $\|\mathbf{A}\|_{\text{F}} = \sqrt{\langle \mathbf{A}, \mathbf{A} \rangle_{\text{F}}}$, respectively, where $(\cdot)^*$ denotes the complex conjugate. Further, 2-norm is given by $\|\mathbf{a}\| = \sqrt{\mathbf{a}^{\text{T}}\mathbf{a}}$. We use the superscripts $(\cdot)^{\text{T}}$ and $(\cdot)^{\text{H}}$ for transposed and Hermitian transposed, respectively.

II. Measurement Setup

The measurement setup is described in [13], [14] and consists of a moving TX and a static receiver (RX). The moving TX is based on an antenna moving along the predefined trajectory around a rotation axis at a constant velocity [15]. The TX is mounted on a sliding board that can be moved in the range of 33 cm and 81 cm along the x and y-axis, respectively. This TX shift allows for measurements to be performed at multiple spatial positions in the sub-6 GHz and mmWave bands. We use horn antennas with half-power beamwidth (HPBW) of 30° at the RX and monopole antennas at the TX for both frequency bands. This allows reproducible measurements and direct comparison of the measured wireless channel in terms of fading environment and channel statistics. The reproducibility of the measurement setup is quantified in [16].

A. Measurement Campaign

Performing repeatable measurements is not feasible in real vehicular scenarios because of the dynamic scattering environment. Therefore, we opt for a measurement in a controlled indoor laboratory environment as shown in Fig. 1. The TX antenna is moving at the rotary unit at a velocity of 100 km/h (see Fig. 3). The channel is recorded on a 1.4 m long trajectory as the TX travels across the arc segment from $-40°$ to $40°$. By taking just a segment of an arc, we have a high-speed, approximately translatory motion, characteristic for vehicular scenarios. Here, we focus on multiband channel characteristics comparison, under high-velocity movement. The RX antenna is placed 7.5 m away from the TX antenna and is static on a laboratory table. For a fair multi-band comparison and reproducibility of the measurement scenarios, the fading environment is kept static with no people or moving objects in the room during the measurements.

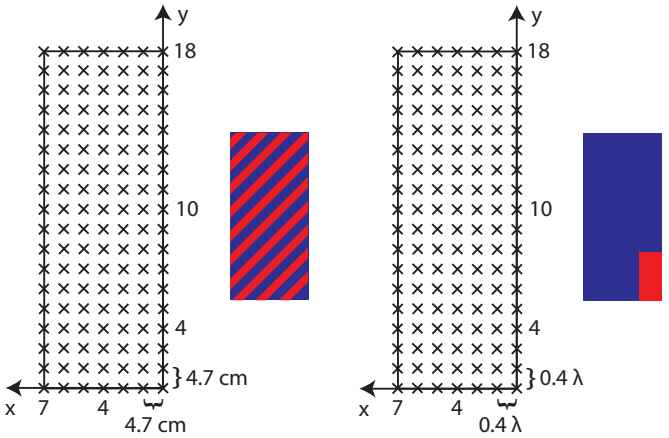

(a) Measurement I: Positions are mutually separated by 4.7 cm to obtain a fair comparison in terms of antenna positions.

(b) Measurement II: Positions are mutually separated by 0.4 λ to obtain a fair comparison in terms of wavelength.

Fig. 2: Detailed view of measured positions. The sub-6 GHz and mmWave positions are represented by blue and red color, respectively.

We conduct measurements at center frequencies of 2.55 GHz (sub-6 GHz) and 25.5 GHz (mmWave) and different spatial positions according to the two rectangular grids, where $x \in \{0, \ldots, N_{\text{x}} - 1\}$ and $y \in \{0, \ldots, N_{\text{y}} - 1\}$ as shown in Fig. 2. Firstly, we conduct measurements at 126 different TX positions, where the positions on the x- and y-axis are mutually separated by 4.7 cm, as shown in Fig. 2a. The blue and red rectangles indicate the measured region for sub-6 GHz, and mmWave, respectively. In this case, TX antenna traces (paths) are identical for sub-6 GHz and mmWave and we obtain a fair comparison in terms of antenna position as described in [17]. Secondly, we perform measurements at 126 different TX positions that are mutually separated by 0.4 λ as shown in Fig. 2b. Here, the positions of the TX antennas for sub-6 GHz and mmWave are not identical, but the separation between the positions is equal in terms of wavelength, as given in [18]. Thereby, we obtain a fair comparison of wireless channels in terms of wavelength.

After performing the measurement and post-processing, as described in [17], we obtain a time-variant channel transfer function $\mathbf{H}_{S \times Q}$, with S and Q samples in the time and

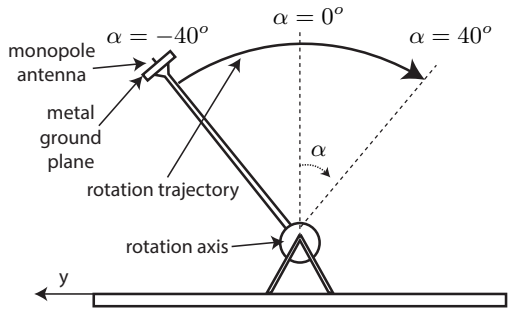

Fig. 3: Rotary trajectory of the TX.

frequency domain, respectively.

III. Stationarity Evaluation

A wireless channel is described by its channel transfer function, $\mathbf{H} \in \mathbb{C}^{S\times Q}$, with sampling time and frequency denoted as T_s and f_s. Since the assumption of stationarity for non-wide-sense stationary uncorrelated scattering (WSSUS) channels is not fulfilled in general, we sequence the channel transfer function in subregions over which we assume the stationarity a priori. We denote these subregions as local channel transfer functions (LCTFs) $\mathbf{H}^{(k_\mathrm{t})}$, of N and M samples in the time and frequency domain over which WSSUS is fulfilled approximately. Here, k_t denotes the index of each LCTF

$$k_\mathrm{t} \in [1, \cdots, K_\mathrm{t}], \;\; K_\mathrm{t} = \left\lfloor \frac{S-N}{\Delta_t} \right\rfloor + 1, \tag{1}$$

with time shift $\Delta_\mathrm{t} T_\mathrm{s}$ between two consecutive LCTFs.

In order to minimize the variance of the spectral estimate, we use a multitaper spectral estimator by applying two-dimensional spectral window functions, based on discrete prolate spheroidal sequence (DPSS) [19],

$$\hat{\mathbf{H}}^{(k_\mathrm{t},w)} = \mathbf{H}^{(k_\mathrm{t})} \odot \mathbf{G}^{(w)}. \tag{2}$$

$\mathbf{G}^{(w)} = \mathbf{s}^{(u)\mathrm{T}} \tilde{\mathbf{s}}^{(v)}$, where $u \in [1, \cdots, I]$, $v \in [1, \cdots, J]$ denotes the window function. $\mathbf{s}^{(u)}$ and $\tilde{\mathbf{s}}^{(v)}$ are DPSSs, described by the energy concentration bandwidth defined as a multiple of the fundamental frequency ($2W_\mathrm{t}$, $2W_\mathrm{f}$), and the number of sequences (I, J), in the time and frequency domain, respectively. The described approach generates time-frequency (TF) limited spectral estimates with low sidelobes.

We estimate the windowed Doppler-variant impulse response $\hat{\mathbf{S}}^{(k_\mathrm{t},w)} = \mathbf{F}_N \hat{\mathbf{H}}^{(k_\mathrm{t},w)} \mathbf{F}_M^H$. By uniform weighting over the estimated windowed Doppler-variant impulse responses we estimate the local scattering function (LSF)

$$\hat{\mathbf{C}}^{(k_\mathrm{t})} = \frac{1}{IJ} \sum_{w=1}^{IJ} \left| \hat{\mathbf{S}}^{(k_\mathrm{t},w)} \right|^2. \tag{3}$$

Further, we estimate the DSD at the $k_\mathrm{t}^{\mathrm{th}}$ time instance

$$\hat{\mathbf{p}}_\nu^{(k_\mathrm{t})} = \frac{1}{M} \hat{\mathcal{C}}^{(k_\mathrm{t})} \mathbf{1}_{M\mathrm{x}1}. \tag{4}$$

By $\hat{\mathbf{P}}_\nu = [\hat{\mathbf{p}}_\nu^{(1)}, \cdots, \hat{\mathbf{p}}_\nu^{(K_\mathrm{t})}]$ we denote the time-dependent DSD, defined over the predefined rotation trajectory.

A. Spatial Stationarity for Predefined TX Movement

In order to observe if the channel stays stationary as the rotation axis of TX moves along the x and y-axis by $(\Delta x, \Delta y)$, we estimate the variation of DSD in the spatial domain. By $\hat{\mathbf{P}}_\nu^{(x,y)}$, we denote the DSD, of the channel when the rotation axis is at the position (x, y) and the TX makes the movement along the predefined trajectory. For a numerical representation of the DSD variation, we introduce a metric collinearity, bounded in the range [0,1], where the value 1 shows identity between the compared DSDs,

$$\gamma[\Delta x, \Delta y] = \frac{1}{U[\Delta x, \Delta y]} \cdot \sum_{\substack{x_\mathrm{r}\in\mathbf{x}^{(\Delta x)};\\ y_\mathrm{r}\in\mathbf{y}^{(\Delta y)}}} \frac{\langle \hat{\mathbf{P}}_\nu^{(x_\mathrm{r},y_\mathrm{r})}, \hat{\mathbf{P}}_\nu^{(x_\mathrm{r}+\Delta x, y_\mathrm{r}+\Delta y)} \rangle_\mathrm{F}}{\sqrt{\left\| \hat{\mathbf{P}}_\nu^{(x_\mathrm{r},y_\mathrm{r})} \right\|_\mathrm{F}^2 \cdot \left\| \hat{\mathbf{P}}_\nu^{(x_\mathrm{r}+\Delta x, y_\mathrm{r}+\Delta y)} \right\|_\mathrm{F}^2}}, \tag{5}$$

where $\mathbf{U}$ is the normalization matrix, defined by the number of possibilities for each $(\Delta x, \Delta y)$ shift

$$U[\Delta x, \Delta y] = (N_\mathrm{x} - |\Delta x| + 1)\,(N_\mathrm{y} - |\Delta y| + 1)\,. \tag{6}$$

The TX shift is in the range $\Delta x \in [-N_\mathrm{x}+1, \cdots, N_\mathrm{x}-1]$, $\Delta y \in [-N_\mathrm{y}+1, \cdots, N_\mathrm{y}-1]$. Furthermore, the values of $\mathbf{x}^{(\Delta x)}$ and $\mathbf{y}^{(\Delta y)}$ are defined as

$$\mathbf{x}^{(\Delta x)} = \begin{cases} [0, \cdots, N_\mathrm{x}], & \forall\ \Delta x \in [0, N_\mathrm{x}-1] \\ |\Delta x|, \cdots, N_\mathrm{x}, & \forall\ \Delta x \in [-N_\mathrm{x}+1, 0[, \end{cases} \tag{7}$$

$$\mathbf{y}^{(\Delta y)} = \begin{cases} [0, \cdots, N_\mathrm{y}], & \forall\ \Delta y \in [0, N_\mathrm{y}-1] \\ [|\Delta y|, \cdots, N_\mathrm{y}], & \forall\ \Delta y \in [-N_\mathrm{y}+1, 0[. \end{cases} \tag{8}$$

We define channel spatial stationary, based on the maximum spatial shift of the TX rotation axis for which the collinearity is above the cut-off value

$$\zeta[\Delta x, \Delta y] = \begin{cases} 1, & \forall\ \gamma[\Delta x, \Delta y] \geq 0.9 \\ 0, & \text{otherwise.} \end{cases} \tag{9}$$

B. Influence of the Antenna Orientation on the Spatial Stationarity

Here, we want to examine how the orientation of the TX antenna influences the spatial stationarity. As the TX moves along the rotary trajectory, the antenna orientation changes as well. Therefore, we select the extreme positions along the path and evaluate the spatial DSD variation. We introduce the metric correlation coefficient ρ, where a value of one shows the identity of the compared vectors. For each selected antenna orientation, defined by the center of the k_t^{th} LCTF definition region, we calculate the correlation coefficient as

$$\rho^{(k_\mathrm{t})}[\Delta x, \Delta y] = \frac{1}{U[\Delta x, \Delta y]} \cdot \sum_{\substack{x_\mathrm{r}\in\mathbf{x}^{(\Delta x)};\\ y_\mathrm{r}\in\mathbf{y}^{(\Delta y)}}} \frac{\hat{\mathbf{p}}_\nu^{(k_\mathrm{t};x_\mathrm{r},y_\mathrm{r})\mathrm{T}} \hat{\mathbf{p}}_\nu^{(k_\mathrm{t};x_\mathrm{r}+\Delta x, y_\mathrm{r}+\Delta y)}}{\left\| \hat{\mathbf{p}}_\nu^{(k_\mathrm{t};x_\mathrm{r},y_\mathrm{r})} \right\|^2 \left\| \hat{\mathbf{p}}_\nu^{(k_\mathrm{t};x_\mathrm{r}+\Delta x, y_\mathrm{r}+\Delta y)} \right\|^2}. \tag{10}$$

IV. Numerical Results

A. Spatial Stationarity for Predefined TX Movement

We evaluate the spatial channel stationarity for a high-velocity scenario by analyzing the channel measurements described as given in Section II. The rotary axis moves along the x and y-axis, taking 126 spatial positions. At each (x, y) position of the rotary axis, we measure the channel as the TX moves along the rotation trajectory ($\alpha \in [-40^o, 40^o]$), and estimate the DSD, $\hat{\mathbf{P}}_\nu^{(x,y)}$. We evaluate the spatial stationarity by calculating collinearity (Eq. (5)) between the estimated DSDs, as the rotary axis moves in the x-y domain by (Δx, Δy).

Estimating DSD starts with specifying the LCTF over a specific number of symbols in the time domain, N. Here, a tradeoff has to be made - choosing higher N, provides a better DSD Doppler resolution but increases the risk of violation stationarity within one LCTF. For estimating the DSD in the 25.5 GHz band, we set $N = 25$ (2.5 ms) samples in the time domain. As the center frequency decreases, the Doppler shift

decreases proportionately. Therefore, we define the LCTF over $N = 100$ samples (10 ms), to keep the Doppler resolution on a comparable level. We opt not to increase the LCTF time span further in order to avoid risking the violation of the WSUS assumption. By adopting the size of LCTF to provide better LSF resolution, we allow for fair multiband comparison in order to investigate the influence of the frequency-selective propagation mechanisms. For all evaluations, we set the LCTF over the whole measured bandwidth, $B = 100\,\text{MHz}$ ($M = 100$), $\Delta_t = 2$, and DPSS window function with the following specification: $W_\text{t} = 1, W_\text{f} = 2, I = 2, J = 3$.

First, we observe the channel impulse responses obtained in the measurement campaign I, where the sub-6 GHz and mmWave channels measurement positions are mutually separated by 4.7 cm (see Fig. 4 and Fig. 5). We observe larger spatial stationarity in the case of sub-6 GHz. Furthermore, both frequency bands show longer stationarity when the rotation axis is shifted in the x than in the y direction. This is due to the specific scenario, where the movement in the y direction means moving closer or away from the door (Fig. 1). Here, the position of the door plays a significant role, as strong channel components originate as a diffraction around the door frame, as shown in [17]. We observe that the sub-6 GHz channels, measured as the TX moves along the predefined trajectory, are stationary for the shift of the trajectory axis in the order of 400 mm in the y, corresponding to 3.4 λ, and at least 300 mm in the x direction. On the other side, mmWave channels show stationarity over the spatial shift of 47 mm in the y, and under 47 mm in the x direction. Here, we notice the requirement for a better spatial resolution of the stationarity investigation in the mmWave domain.

In order to investigate spatial stationarity scalability with the center frequency, measurement II is performed, where the measurement positions are chosen with 0.4λ separation with respect to the center frequency. The measurement grid for sub-6 GHz stays unchanged, and the mmWave measurement grid is downscaled by a factor of 10, providing a better spatial resolution. Comparing Fig. 5 and Fig. 6 we conclude, the spatial stationarity under the predefined rotary movement for 25.5 GHz band is in the order of 30 mm in the y, corresponding to 2.5 λ and 47 mm in the x direction. From this measurement we hence conclude that the spatial stationarity region is approximately downscaled with the increased center frequency for this scenario.

B. Influence of the Antenna Orientation on the Spatial Stationarity

While the RX antenna is static for all measurements, the TX antenna has a different orientation as it moves along the rotation trajectory. We compare the channels estimated over the trajectory segment of 4.00^o, centered at *a)* $\alpha = -38^o$, *b)* $\alpha = 0^o$ and *c)* $\alpha = 38^o$ (Fig. 3). For each of the three TX orientations, we obtain the correlation coefficient of the DSDs as the TX makes a spatial shift by $(\Delta x, \Delta y)$. Fig. 7 shows the cumulative distribution function (CDF) of the correlation coefficient for the three TX orientations. We can notice that the TX orientation $\alpha = 0^o$ shows the highest

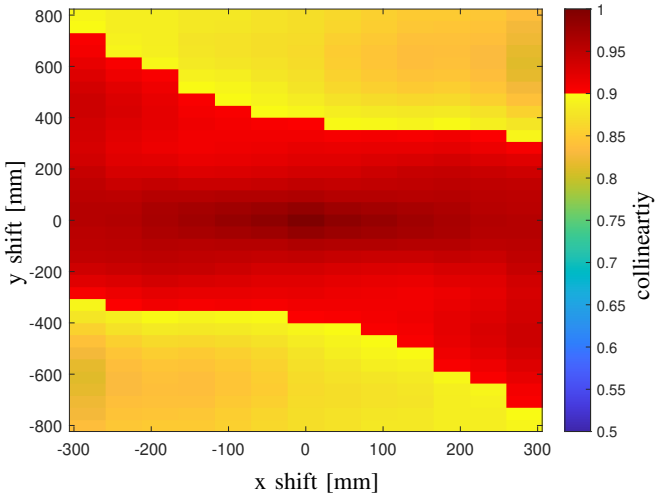

Fig. 4: Stationarity evaluation for $\text{f}_\text{c} = 2.55\,\text{GHz}$.

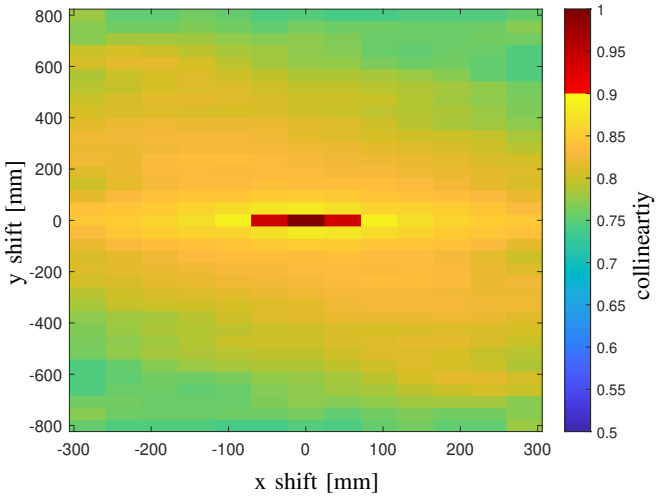

Fig. 5: Stationarity evaluation for $\text{f}_\text{c} = 25.5\,\text{GHz}$; measurement I.

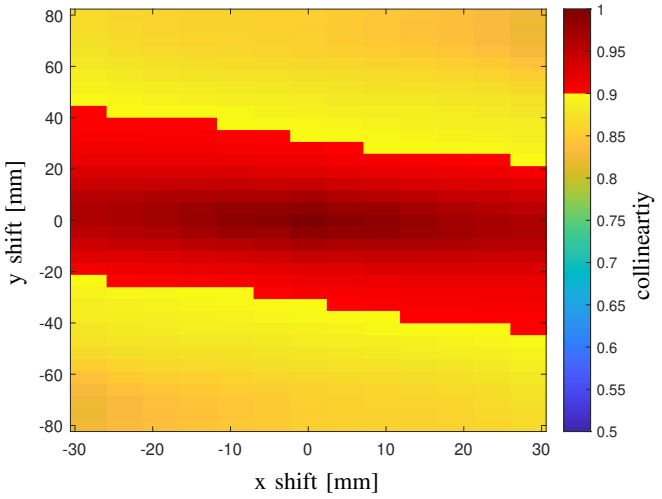

Fig. 6: Stationarity evaluation for $\text{f}_\text{c} = 25.5\,\text{GHz}$; measurement II.

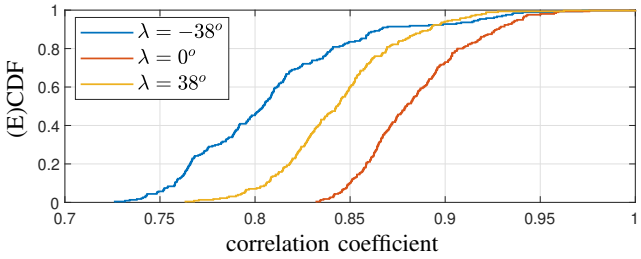

Fig. 7: Stationarity evaluation dependent on TX antenna orientation, $f_c = 25.5$ GHz.

values of DSD spatial correlation, followed by $\alpha = 38^o$. This is to be understood by discussing the TX and RX positioning and the measurement environment (Fig. 1). When the TX is at the position $\alpha = 0^o$ its radiation pattern aligns with the main lobe of the RX antenna, hence the strongest component propagates directly through a thin brick wall A. The presence of a single dominant channel component enlarges stationarity, as shown in [11]. Furthermore, for the orientation $\alpha = 38^o$, TX is oriented towards the door, allowing for diffraction around the door frame. Therefore, the strong diffraction component dominates the channel, enlarging the stationarity region. As the TX takes the position $\alpha = -38^o$, it is tilted away from the door and TX and RX antennas are misaligned, allowing for multiple attenuated reflections of wall B to reach the RX, without a dominating channel component.

V. Conclusion

In this paper, we evaluated the spatial channel stationarity for a high-velocity multi-band scenario. We investigated the channels in the 2.55 GHz and 25.5 GHz frequency bands, measured at 126 positions in the spatial domain. For each position, the channel is measured while the TX moves along a perfectly identical trajectory, with a velocity of 100 km/h. We estimated the DSD for each position and evaluated its variation as the rotary axis makes a shift in the two-dimensional space. We, estimated the spatial stationarity in the order of $400\,\text{mm} = 3.4\,\lambda$ for 2.55 GHz and $30\,\text{mm} = 2.5\,\lambda$ for 25.5 GHz frequency band for our chosen scenario. Hence, the spatial stationarity is proportional to the wavelength. Finally, we showed that the antenna orientation influences the spatial stationarity, by filtering specific channel components. We showed that the presence of dominant channel components contributes to larger spatial stationarity.

References

[1] "Final report of the single platform for open road testing and predeployment of cooperative, connected and automated and autonomous mobility platform (CCAM Platform)," European Commission, Directorate-General for Mobility and Transport, Tech. Rep., 07 2021, [Online]. Available: https://transport.ec.europa.eu/transport-themes/intelligent-transport-systems/cooperative-connected-and-automated-mobility-ccam_en.

[2] C. F. Mecklenbrauker, A. F. Molisch, J. Karedal, F. Tufvesson, A. Paier, L. Bernado, T. Zemen, O. Klemp, and N. Czink, "Vehicular Channel Characterization and Its Implications for Wireless System Design and Performance," *Proceedings of the IEEE*, vol. 99, no. 7, pp. 1189–1212, 2011.

[3] R. Hadani, S. Rakib, M. Tsatsanis, A. Monk, A. J. Goldsmith, A. F. Molisch, and R. Calderbank, "Orthogonal Time Frequency Space Modulation," in *2017 IEEE Wireless Communications and Networking Conference (WCNC)*, 2017, pp. 1–6.

[4] K. R. Murali and A. Chockalingam, "On OTFS Modulation for High-Doppler Fading Channels," in *2018 Information Theory and Applications Workshop (ITA)*, 2018, pp. 1–10.

[5] T. Zemen, M. Hofer, D. Loeschenbrand, and C. Pacher, "Iterative detection for orthogonal precoding in doubly selective channels," in *IEEE International Symposium on Personal, Indoor and Mobile Radio Communications (PIMRC)*, Bologna, Italy, September 2018.

[6] P. Raviteja, E. Viterbo, and Y. Hong, "OTFS Performance on Static Multipath Channels," *IEEE Wireless Communications Letters*, vol. 8, no. 3, pp. 745–748, 2019.

[7] D. Radovic, C. F. Mecklenbräuker, and T. Blazek, "OTFS Performance Over Different Measured Vehicular 60 GHz Millimeter-Wave Channels," in *2021 International Conference on Software, Telecommunications and Computer Networks (SoftCOM)*, 2021, pp. 1–5.

[8] L. Bernadó, T. Zemen, F. Tufvesson, A. F. Molisch, and C. F. Mecklenbräuker, "The (in-) validity of the WSSUS assumption in vehicular radio channels," in *2012 IEEE 23rd International Symposium on Personal, Indoor and Mobile Radio Communications - (PIMRC)*, 2012, pp. 1757–1762.

[9] M. Yang, B. Ai, R. He, Z. Ma, H. Mi, D. Fei, Z. Zhong, Y. Li, and J. Li, "Dynamic V2V Channel Measurement and Modeling at Street Intersection Scenarios," *IEEE Transactions on Antennas and Propagation*, vol. 71, no. 5, pp. 4417–4432, 2023.

[10] J.-J. Park, J. Lee, K.-W. Kim, M.-D. Kim, H.-K. Kwon, and K. C. Lee, "Wide-Sense Stationarity of Millimeter Wave Expressway Channels Based on 28 GHz Measurements," in *2019 IEEE 90th Vehicular Technology Conference (VTC2019-Fall)*, 2019, pp. 1–5.

[11] D. Radovic, H. Groll, and C. F. Mecklenbräuker, "Evaluation of stationarity regions in measured non-WSSUS 60 GHz mmWave V2V channels," in *2022 56th Asilomar Conference on Signals, Systems, and Computers*, 2022, pp. 1212–1216.

[12] D. Radovic, F. Pasic, M. Hofer, H. Groll, C. F. Mecklenbräuker, and T. Zemen, "Stationarity Evaluation of High-mobility sub-6 GHz and mmWave non-WSSUS Channels," in *2023 XXXVth General Assembly and Scientific Symposium of the International Union of Radio Science (URSI GASS)*, 2023, pp. 1–4.

[13] F. Pasic, S. Pratschner, R. Langwieser, D. Schützenhöfer, E. Jirousek, H. Groll, S. Caban, and M. Rupp, "Sub 6 GHz versus mmWave Measurements in a Controlled High-Mobility Environment," in *WSA 2021; 25th International ITG Workshop on Smart Antennas*, 2021.

[14] F. Pasic, D. Schützenhöfer, E. Jirousek, R. Langwieser, H. Groll, S. Pratschner, S. Caban, S. Schwarz, and M. Rupp, "Comparison of Sub 6 GHz and mmWave Wireless Channel Measurements at High Speeds," in *16th European Conference on Antennas and Propagation (EuCAP 2022)*, 2022.

[15] S. Caban, J. Rodas, and J. A. García- Naya, "A methodology for repeatable, off-line, closed-loop wireless communication system measurements at very high velocities of up to 560 km/h," in *2011 IEEE International Instrumentation and Measurement Technology Conference*, 2011.

[16] F. Pasic, M. Hofer, D. Radovic, H. Groll, S. Caban, T. Zemen, and C. F. Mecklenbräuker, "Quantifying the Reproducibility of Multi-Band High Speed Wireless Channel Measurements," in *2023 IEEE 34rd Annual International Symposium on Personal, Indoor and Mobile Radio Communications (PIMRC)*, 2023. [Online]. Available: https://thomaszemen.org/papers/Pasic23-PIMRC-paper.pdf

[17] F. Pasic, M. Hofer, M. Mussbah, H. Groll, T. Zemen, S. Schwarz, and C. F. Mecklenbräuker, "Statistical Evaluation of Delay and Doppler Spreads in sub-6 GHz and mmWave Vehicular Channels," in *2023 IEEE 97th Vehicular Technology Conference (VTC2023-Spring)*, 2023.

[18] F. Pasic, N. Di Cicco, M. Skocaj, M. Tornatore, S. Schwarz, C. F. Mecklenbräuker, and V. Degli-Esposti, "Multi-Band Measurements for Deep Learning-Based Dynamic Channel Prediction and Simulation," *IEEE Communications Magazine*, vol. 61, no. 9, pp. 98–104, 2023.

[19] D. Slepian, "Prolate Spheroidal Wave Functions, Fourier Analysis, and Uncertainty-V: The Discrete Case," *Bell Syst. Techn J.*, vol. 57, no. 5, pp. 1371–1430, May 1978.